

Vibrational signatures of HNO₃ acidity when complexed with microhydrated alkali metal ions, M⁺·(HNO₃)(H₂O)_{n=5} (M=Li, K, Na, Rb, Cs), at 20 K.

Sayoni Mitra^a, Thien Khuu,^a Tae Hoon Choi,^b Rachel M. Huchmala,^c

Kenneth D. Jordan,^b Anne B. McCoy^c and Mark A. Johnson^a

^aSterling Chemistry Laboratory, Yale University, New Haven, CT, 06520, USA

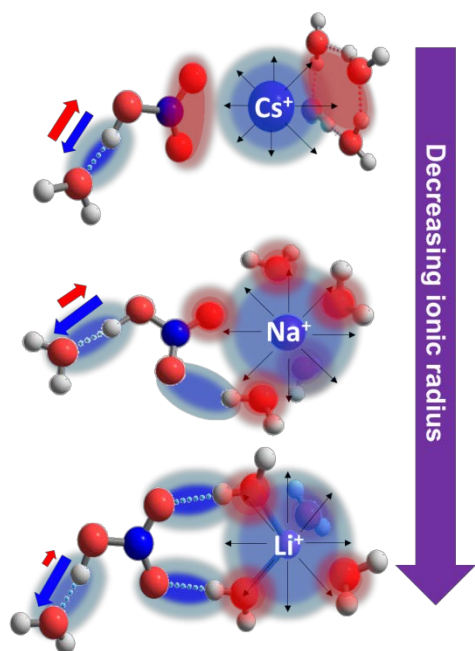
^bDepartment of Chemistry, University of Pittsburgh, PA, 15260, USA

^cDepartment of Chemistry, University of Washington, Seattle, WA 98195, USA

Abstract

The speciation of strong acids like HNO₃ under conditions of restricted hydration is an important factor in the rates of chemical reactions at the air-water interface. Here we explore the trade-offs in play when HNO₃ is attached to alkali ions (Li⁺-Cs⁺) with four water molecules in their primary hydration shells. This is achieved by analyzing the vibrational spectra of the M⁺·(HNO₃)(H₂O)₅ clusters cooled to about 20 K in a cryogenic photofragmentation mass spectrometer. The local acidity of the acidic OH group is estimated by the extent of the red shift in its stretching frequency when attached to a single water molecule. The persistence of this local structural motif (HNO₃-H₂O) in all of these alkali metal clusters enables us to determine the competition between the effect of the direct complexation of the acid with the cation, which acts to enhance acidity, and the role of the water network in the first hydration shell around the ions, which acts to counter (screen) the intrinsic effect of the ion. Analysis of the vibrational features associated with the acid molecule as well as those of the water network reveal how cooperative interactions in the micro hydration regime conspire to effectively offset the intrinsic enhancement of HNO₃ acidity afforded by attachment to the smaller cations.

TOC Graphic



I. Introduction

The unusual behavior of HNO₃ at the air-water interface is currently under investigation with a variety of theoretical and experimental methods.¹⁻¹⁰ Specifically, it has been proposed that this strong acid (under typical aqueous conditions) is only partially ionized near the water surface where the counter ions are less efficiently solvated.^{1,3,6} Understanding the nature of aqueous HNO₃ in pure water as well as in the presence of electrolytes has motivated several theoretical and experimental efforts designed to establish how its pK_a depends on the local environment.¹¹⁻¹³ These involve elucidation of HNO₃ behavior at the air-water interface as well as in well-defined cluster systems (e.g., Cs⁺·(HNO₃)(H₂O)_{n=0-11}).^{4,14-16} The advantage of the cluster regime is that electronic structure calculations can be applied to harvest the structural information encoded in experimental vibrational band patterns obtained with size-selective, cryogenic photofragmentation mass spectrometry.¹⁷ Using this approach, for example, Mitra et al.¹⁶ recently observed the cluster-size-dependent onset of the solvent-separated, NO₃⁻/H₃O⁺ ion pair in the ~20 K Cs⁺·(HNO₃)(H₂O)_n system at n~10. Calculations revealed the critical role played by the proximal Cs⁺ ion to stabilize the incipient NO₃⁻ conjugate base in a water network-mediated, Cs⁺/NO₃⁻/H₃O⁺ salt bridge arrangement. This raises a long standing issue in aqueous chemistry dating back to the seminal work of Fuoss and Onsager¹⁸ in the 1930s regarding the dependence of an acid's pK_a value on ionic strength of a solution. The presence of alkali ions in water clusters, for example, has been shown to decrease the proton mobility displayed by pure water clusters,¹⁹ and simulations indicated that anions like Cl⁻ enhance acidity of HNO₃ in the Cl⁻·(HNO₃)(H₂O)₂₀ cluster.¹³

One way to gauge the acidity of an acid is to monitor the red-shift in the acidic OH stretching fundamental (hereafter denoted $\nu_{\text{OH}}^{\text{a-w}}$) when it is attached to a common base.²⁰ In the case of the Cs⁺·(HNO₃)(H₂O)_n system, clusters formed by electrospray ionization can occur with one water molecule

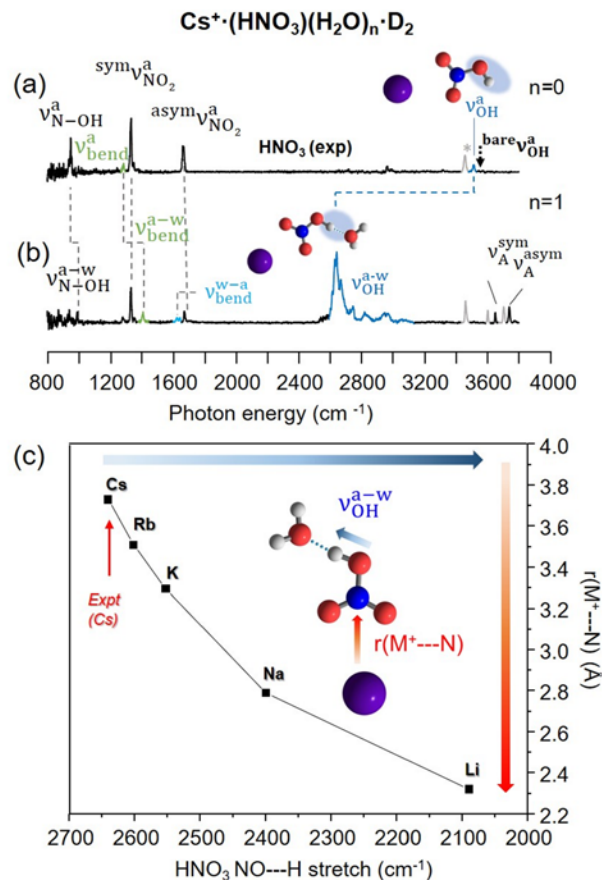


Figure 1: Traces (a) and (b) show predissociation spectra of Cs⁺·HNO₃·D₂ and Cs⁺·(HNO₃)(H₂O)·D₂, reproduced from reference 15. All band labels aid referencing in the text and **Tables S1 and S2**. Bands colored grey are due to isomers arising from the tag location in (a) and the water molecule in (b). Plot (c) depicts the trend between the calculated acid OH stretch ($\nu_{\text{OH}}^{\text{a-w}}$) and M⁺---N bond distance ($r(\text{M}^{\text{+}}\text{---N})$) for M⁺·(HNO₃)(H₂O), M=Cs, Rb, K, Na and Li. These results were obtained using the B3LYP density functional method, as described in the text and Section S1. The calculated harmonic acid OH frequencies have been scaled by a factor of 0.9, as explained in **Figure S7**. The red arrow in (c) marks the experimental frequency $\nu_{\text{OH}}^{\text{a-w}}$ measured for Cs⁺·(HNO₃)(H₂O)·D₂.¹⁵ The inset provides a representative structural motif of the M⁺·(HNO₃)(H₂O) complex investigated in this study.

attached to the acid while the remaining waters reside in the first hydration shell of the ion.¹⁵⁻¹⁶ For the $n=1$ system, the key bands and structure of this ternary complex are indicated in **Fig. 1b**, where a red-shift of 867 cm^{-1} is observed for $\nu_{\text{OH}}^{\text{a-w}}$ relative to the value in the bare ion $\text{Cs}^+\cdot(\text{HNO}_3)$ (blue, $\nu_{\text{OH}}^{\text{a}}$ in **Fig. 1a** and $\nu_{\text{OH}}^{\text{a-w}}$ in **Fig. 1b**).¹⁵ To put this in context, addition of a water molecule to HNO_3 in carbon tetrachloride⁷ causes the OH stretch to red-shift relative to the solvated acid OH stretch ($\nu_{\text{OH}}^{\text{a}}(\text{CCl}_4)$) by only $\sim 400\text{ cm}^{-1}$. Thus, addition of the Cs^+ ion to neutral $\text{HNO}_3(\text{H}_2\text{O})$ to form the ternary $\text{Cs}^+\cdot(\text{HNO}_3)(\text{H}_2\text{O})$ complex further red-shifts the band by 459 cm^{-1} ,^{15,21} reflecting the enhancement of HNO_3 acidity by the proximal ion. This local $\text{HNO}_3\text{-H}_2\text{O}$ motif was observed to persist up to $n=6$ in the $\text{Cs}^+\cdot(\text{HNO}_3)(\text{H}_2\text{O})_n$ system, and the $\nu_{\text{OH}}^{\text{a-w}}$ band was observed to gradually blue shift back toward the bare value as water molecules were added to the first hydration shell of the ion.¹⁶ Since the fundamental cause for this shift is traced to the electric field generated by the ion, one question raised by that observation is how the $\nu_{\text{OH}}^{\text{a-w}}$ red shift depends on the ionic radius of the metal ion, since smaller ions tend to be closer to the functional group of interest and therefore place this functional group, in this case the acidic OH group, in a region with larger field. This effect is illustrated in **Fig. 1c**, where we show the calculated (scaled by 0.9) harmonic $\nu_{\text{OH}}^{\text{a-w}}$ fundamentals for the ternary alkali ion complexes. Indeed, the introduction of the smaller ions are predicted to cause much larger $\nu_{\text{OH}}^{\text{a-w}}$ red shifts, which are strongly correlated with the distance between the metal ion and the N atom ($r_{\text{M}^+\text{---N}}$). From a physical perspective, decreasing the $\text{M}^+\text{---N}$ distance increasingly stabilizes the incipient $\text{NO}_3^{\delta-}$ moiety that will become the conjugate base upon complete dissociation. Here we explore how the $\nu_{\text{OH}}^{\text{a-w}}$ feature, shown in blue in **Fig. 1b**, evolves for the $\text{M}^+\cdot(\text{HNO}_3)(\text{H}_2\text{O})_5$, $\text{M}=\text{Li, Na, K, Rb, Cs}$ series, where the $n=5$ cluster size was selected on the basis that it is the smallest size for which the critical ternary motif shown in **Fig. 1** is present for all five alkali metals. This dependence is measured by recording the vibrational spectra of the D_2 -tagged, mass-selected and cryogenically cooled ions, and analyzing the resulting band patterns in the context of those predicted for various minimum energy structures recovered by electronic structure calculations. These calculations and the others presented in this paper were carried out using the B3LYP²²⁻²³ density functional theory together with effective core potentials for sodium and the heavier alkali atoms. The details of the calculations and justification for the scaling factor are provided Section S1 in the SI.

II. Experimental methods

The $\text{M}^+\cdot(\text{HNO}_3)(\text{H}_2\text{O})_5$ ions were generated by electrospray ionization of the M^+X^- ($\text{M}=\text{Li, K, Na, Rb, Cs}$; $\text{X}=\text{NO}_3/\text{Cl}^-$) solutions in water at 5-10 mM concentrations and then passing the $\text{M}^+\cdot(\text{H}_2\text{O})_n$ clusters through a radiofrequency ion guide filled with pure HNO_3 vapor at a pressure of $\sim 1\text{ mTorr}$. The HNO_3 pressure was optimized for the attachment of one HNO_3 molecule to the clusters, which occurs by ligand exchange with a water molecule. The resulting cluster distributions are presented in **Fig. S1**. Interestingly, the number of water molecules, n , retained in the $\text{M}^+\cdot(\text{HNO}_3)(\text{H}_2\text{O})_n$ product clusters upon HNO_3 incorporation depends strongly on the metal ion, with an onset occurring at larger numbers of water molecules for the smaller ions. This trend can be rationalized by fact that the smaller ions bind water much more strongly than HNO_3 ,²⁴ but the $\text{M}^+\cdot(\text{H}_2\text{O}) + \text{H}_2\text{O}$ dissociation energies (ΔH_n) quickly fall off with increasing n and heavier alkali metals.²⁵⁻²⁶ For example, the dissociation enthalpies for the $\text{M}^+(\text{H}_2\text{O}) \rightarrow \text{H}_2\text{O} + \text{M}^+$ reactions (ΔH_1) have been measured using high pressure mass spectrometry, and increase from 13.7 to 34.0 kcal/mol (1 atm, 298 K) for $\text{M}=\text{Cs}$ and Li , respectively. Correspondingly, for

the $M^+(H_2O)_4 \rightarrow M^+(H_2O)_3 + H_2O$, the enthalpies are 10.6 and 16.4 for Cs and Li.²⁵ In that scenario, the ligand exchange reactions only begin when the HNO_3 binding energy to the cluster is on the same order as that to a water molecule. Once formed, the product ions are transferred to a ~ 20 K ion trap and tagged with D_2 molecules before being injected into a triple-focusing photofragmentation mass spectrometer described in detail previously.^{21, 27} Vibrational spectra are recorded by monitoring IR photodissociation of the D_2 tags in a linear action regime with a pulsed, tunable IR laser (LaserVision OPO/OPA). For the $n=5$ clusters of interest here, we note that secular frequency-induced dissociation (SFID) of the $M^+(HNO_3)(H_2O)_5$ ions resulted primarily in the loss of HNO_3 , consistent with the acid being less strongly bound to the ions than water. In order to perform SFID, the ions were first mass-isolated using an amplitude-modulated (AM) secular frequency sweep applied through one of the end caps of the Paul Trap, where the waveform amplitude is reduced to zero as the sweep frequency approaches the secular frequency of the ion of interest and then restored after the sweep passes this frequency.²⁸ After isolation, a second, resonant AM secular frequency burst is applied to the same Paul Trap to excite and selectively break up the ion of interest. Mass spectra of the dissociation branching ratios are reported in **Figs. S2 and S3**.

III. Results and Discussion

Panels **2b-2e** in **Figure 2** present a summary of the D_2 -tagged $M^+(HNO_3)(H_2O)_5$ spectra obtained in this work, along with that recorded earlier for $Cs^+(HNO_3)(H_2O)_5$ in **Fig. 2a**.¹⁶ There is a complication in interpreting several of these spectra that arises because more than one isomer can be formed, and indeed for $Cs^+(HNO_3)(H_2O)_4$, which is similar to $n=5$ spectrum, two isomers were isolated using two-color, IR-IR hole burning spectroscopy.¹⁶ One of these adopts the ternary motif of primary interest here ($(H_2O)_4 \cdot Cs^+ \cdot HNO_3 \cdot H_2O$, herein denoted isomer **5I**), while the other (herein denoted isomer **5II**) occurs with a water molecule added to the second hydration shell (SS) of the acid OH group in an H-bond acceptor (A) configuration as indicated in the inset in **Fig. 2c**. Spectral features associated with **5II** are highlighted in orange. The presence of the resulting AD water in the SS motif is clearly evidenced by the appearance of a telltale band (${}^3w_{MAD}^{bound}$) near 3335 cm^{-1} that is due to the OH stretch that links the two water molecules together. A second characteristic feature of the AD motif is the band near $\sim 1860\text{ cm}^{-1}$, which arises from the overtone in the out-of-plane (*oop*) displacement of the acidic OH group ($v_{NO_3H}^{2 \times oop}$). This band gains intensity from the large charge redistribution when the hydrogen bond between the acid and the water dimer is partially broken as the OH group moves along the *oop* normal mode.²⁹ Other characteristic bands associated with this SS morphology are indicated in orange. Interestingly, the ${}^3w_{MAD}^{bound}$ band decreases in intensity in the Rb and K spectra and completely disappears in those of the Na and Li clusters (**Fig. 2d** and **2e**, respectively), reflecting a negligible contribution from the **5II** isomer. This effect again reflects the stronger water binding by the smaller ions such that the remote water in the second shell is drawn back into the primary hydration shell around the ions. Note that once the SS isomers are eliminated in the Na and Li clusters, their spectra become simpler, consistent with formation of a single dominate isomeric form with water molecules in the first hydration shell.

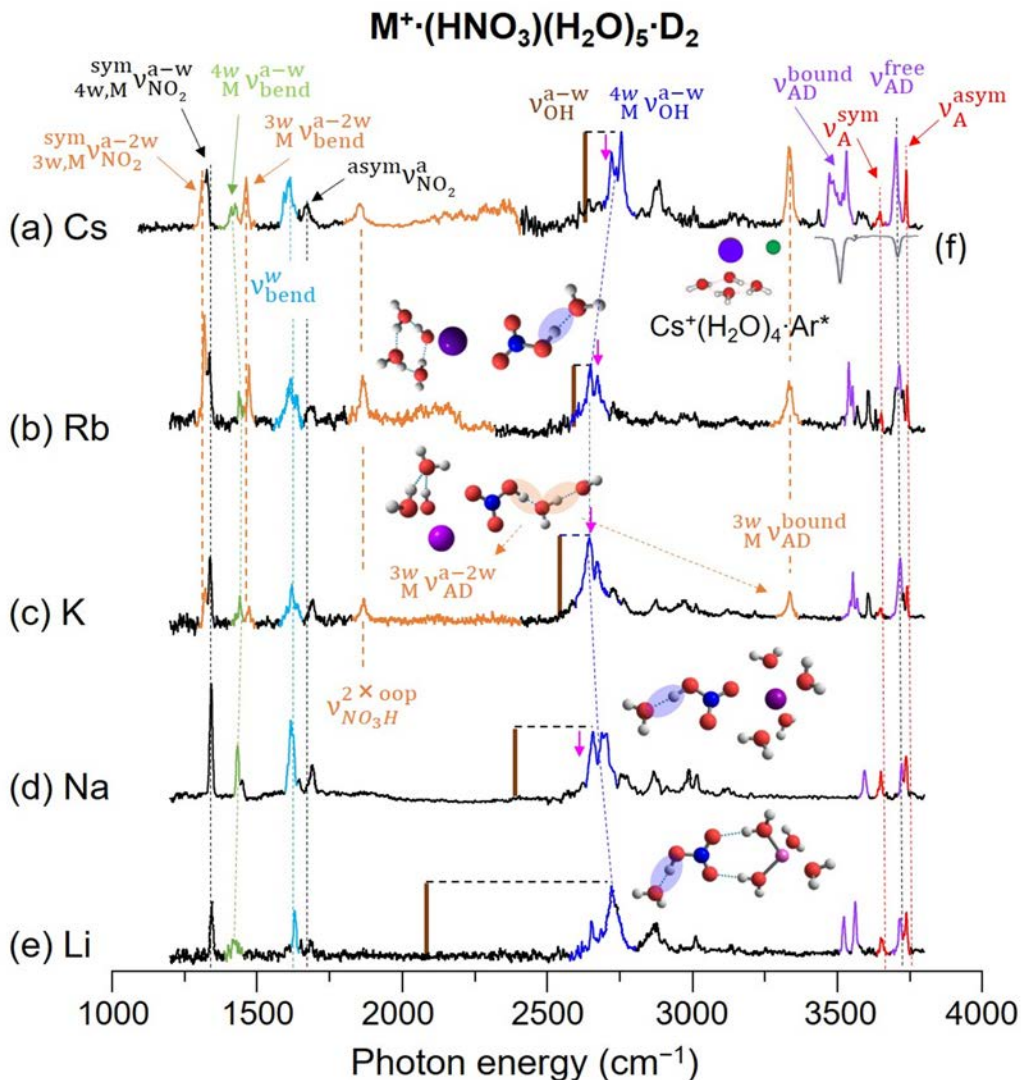


Figure 2: Traces (a)-(e) indicate the vibrational predissociation spectra of D_2 tagged $M^+(\text{HNO}_3)(\text{H}_2\text{O})_5$ ($M = \text{Cs, Rb, K, Na, Li}$) complexes. Trace (f) is the spectrum of $\text{Cs}^+(\text{H}_2\text{O})_4 \cdot \text{Ar}$ obtained from reference 31. The hydrogen bonded acid stretch and bend $\text{NOH}-\text{OH}_2$ (${}^4w_M v_{\text{OH}}^{\text{a-w}}$, navy blue and ${}^4w_M v_{\text{bend}}^{\text{a-w}}$, green) bands are highlighted along with the calculated stick bands for $M^+(\text{HNO}_3)(\text{H}_2\text{O})_1 \cdot D_2$ ($v_{\text{OH}}^{\text{a-w}}$, brown). The bands associated with the AD and A water molecules are highlighted in purple and red, respectively. Features of the **5II** isomer are colored orange and are seen only for $M = \text{Cs, Rb}$ and K . The pink arrows in traces (a)-(d) indicate the calculated ${}^4w_M v_{\text{OH}}^{\text{a-w}}$ peak for the case where the first hydration shell water molecules adopt a cyclic tetramer motif, which is a local minimum for these systems. All band labels aid referencing in the text and **Tables S2, S3 and S4**. The harmonic bands obtained from the B3LYP calculations are scaled by 0.9, as explained in **Fig. S7**. Calculation details are provided in **Section S1**. Structures shown are provided in **Fig. S6**.

All of the $n=5$ clusters are generated with at least one isomer adopting the ternary motif, as evidenced by the strong ${}^4w_M v_{\text{OH}}^{\text{a-w}}$ bands (navy blue) that appear with similar multiplet character to that displayed by Cs. Such spectral complexities are typical for strongly bound OH groups and result from a combination of Fermi resonance interaction with the bend overtone as well as activation of combination

bands with soft modes.²⁹ What is remarkable, however, is the fact that the ${}^4w_M\nu_{\text{OH}}^{\text{a-w}}$ band (navy blue) does not evolve toward lower energy with decreasing size of the alkali ion, as might have been expected for the calculated trend for the $n=1$ systems (**Fig. 1a** and as displayed by brown bars in **Fig. 2**). Rather, the ${}^4w_M\nu_{\text{OH}}^{\text{a-w}}$ band slightly red-shifts from $M = \text{Cs}$ to Rb but then evolves toward *higher* energy from $M = \text{K}$ to Li . Such a non-monotonic evolution is clearly at odds with a simple interpretation that acidity depends on the electric field derived from the alkali ion, and raises the question of the role of the water network in the primary hydration shell. We note that the shifts displayed by the ${}^4w_M\nu_{\text{OH}}^{\text{a-w}}$ and its bending fundamental are observed to be anti-correlated such that lowering ${}^4w_M\nu_{\text{OH}}^{\text{a-w}}$ occurs with increasing ${}^4w_M\nu_{\text{bend}}^{\text{a-w}}$. This trend has been reported earlier,³⁰ and the articulation of it in the present systems is included in **Fig. S4**.

To address the nature of water networks around alkali metal ions, it is useful to recall the extensive body of work on the structures of $M^+(\text{H}_2\text{O})_n$ ions assembled over the past 15 years or so.³¹⁻³³ The general trend is for the formation of cyclic so-called “homodromic” networks bound to larger ions, which reflect the intrinsic structural propensities of neutral water.³⁴⁻³⁶ For smaller ions, however, the hydration numbers describing the local environments in bulk water drop from $n=6-7$ in $\text{Cs}^+(\text{HNO}_3)(\text{H}_2\text{O})_n$ down to 4 for $\text{Li}^+(\text{HNO}_3)(\text{H}_2\text{O})_5$.³⁷ In the cluster regime, this manifests as an ion-induced breakup of the cyclic structures as the water molecules are forced to align closer to the electric dipole direction that bifurcates the symmetry axis. The lowest energy structures of the $n=4$ clusters are presented in **Fig. S5**. For the $\text{Cs}^+(\text{H}_2\text{O})_4$ cluster, the cyclic tetramer is the lowest energy form, as evidenced by the comparison of the $\text{Cs}^+(\text{HNO}_3)(\text{H}_2\text{O})_5$ spectrum in **Fig. 2a** with that of the $\text{Cs}^+(\text{H}_2\text{O})_4$ (inverted) **Fig. 2f**. The tetramer configuration on the ion differs from the neutral water tetramer structure, which has zero dipole moment,³⁸ by having all four free OH groups pointing away from the positive charge center, thereby generating a net-dipole moment in the ion-bound water cluster.

With the $M^+(\text{H}_2\text{O})_n$ structures in mind, we note that the **5I** isomer of $\text{Cs}^+(\text{HNO}_3)(\text{H}_2\text{O})_5$ occurs with the cyclic water tetramer attached to the ion with the $\text{HNO}_3(\text{H}_2\text{O})$ moiety opposite to the cycle as shown at the top of **Fig. 2b**. The modest increase in $\nu_{\text{OH}}^{\text{a-w}}$ ($\sim 107 \text{ cm}^{-1}$ going from $n=1$ to 5) can then be rationalized by considering the competition between the electric field along the acidic OH bond axis, \mathcal{E} , that is due to the ion, \mathcal{E}_{ion} , and that arising from the hydration shell, \mathcal{E}_{hyd} , which reflects the ion-induced orientational and electronic polarizabilities. Note that at the location of the acidic OH group, these fields oppose one another. This effect has been explored in detail in a recent study of the response of the CO stretching bands of a $-\text{CO}_2^-$ head group when bound to the $\text{Ca}^{2+}\cdot\text{CD}_3\text{CD}_2\text{CO}_2^-(\text{H}_2\text{O})_{n=0-15}$ clusters.³⁹ In the classical case of continuum dielectrics, for example, this conforms to the screening regime in which the induced polarization of the medium is opposite in direction and proportional to the field (in the linear response case) from the fixed charge that drives the solvent response.⁴⁰⁻⁴² The interesting aspect of the cluster behavior is, therefore, that it directly explores the trade-offs that drive local electric fields in the vicinity of the ion in the so-called “dielectric saturation” regime.⁴³ That situation arises when the water molecules are essentially locked into position rather than oriented preferentially along field lines while undergoing diffuse rotational motion far from the ion at elevated temperature in the bulk. The calculated ${}^4w_M\nu_{\text{OH}}^{\text{a-w}}$ values for all of the $n=5$ cluster isomers with a tetramer hydration shell motif are indicated by the downward pink arrows in **Fig. 2a-2d**. These shapes are local minima for all the alkalis (except Li), and feature bidentate attachment of the $-\text{NO}_2$ group on the acid to the ion in the first hydration shell. Indeed, the water molecules in the first hydration shell almost completely cancel the large shifts (brown

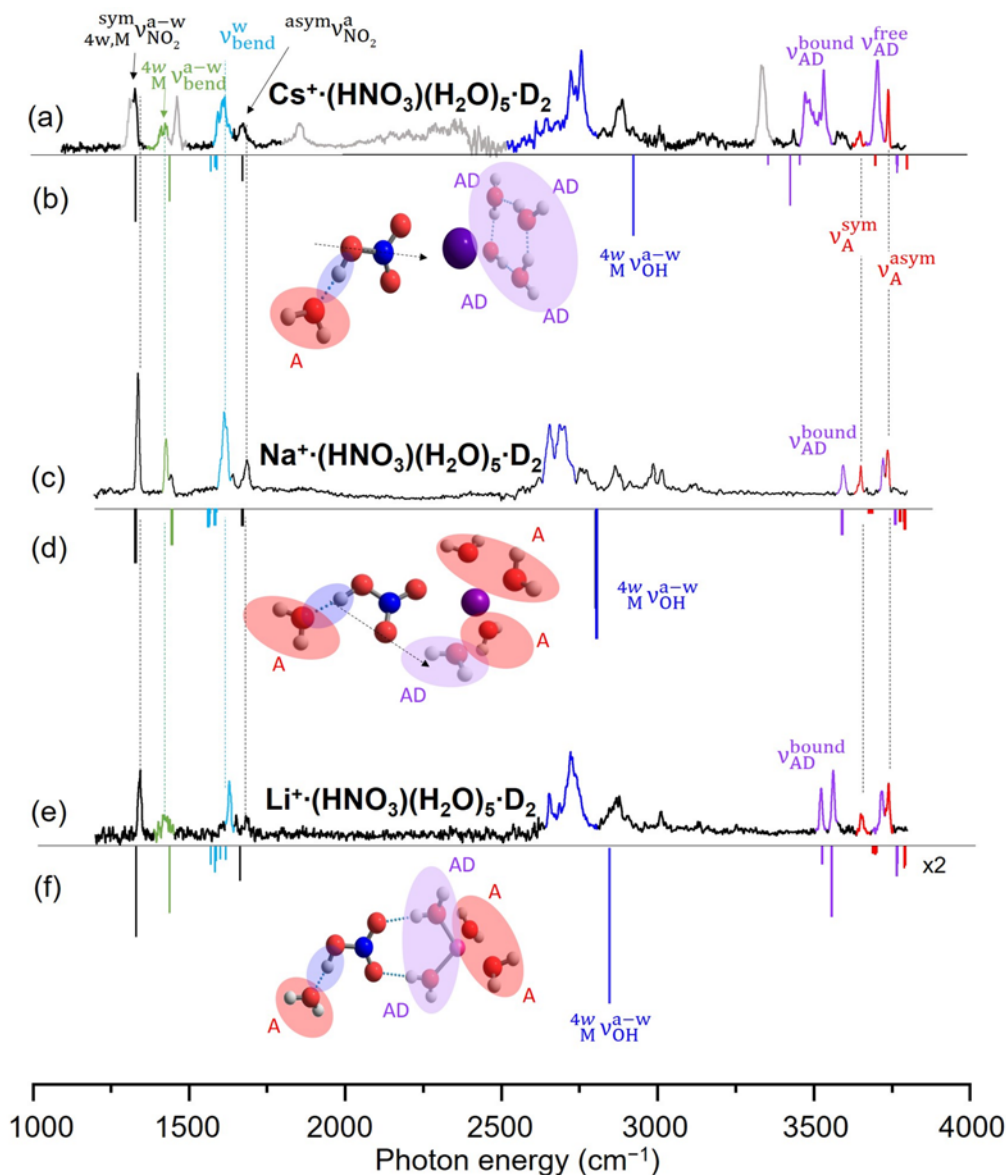


Figure 3: Traces (a), (c), and (e): IR photodissociation of $M^+(\text{HNO}_3)(\text{H}_2\text{O})_5 \cdot \text{D}_2$ ($M = \text{Cs}, \text{Na}, \text{Li}$), along with (b), (d), and (f): calculated minimum energy structures and harmonic spectra with scaling factor of 0.9740 for bands above 1800 cm^{-1} and 0.9719 for bands below 1800 cm^{-1} . Spectrum (a) was obtained and modified from ref. 16. The 0.9740 scaling factor was invoked by normalizing the calculated AD fundamentals to the experimental values. (The 0.9 factor used elsewhere is normalized to the $n=1$ acid OH, $_{\text{Cs}}v_{\text{OH}}^{\text{a-w}}$). A dash arrow bisects the N—OH bond axis to of the Cs^+ and Na^+ structures to highlight the bidentate (Cs^+) versus monodentate (Na^+) interactions between nitric acid and the metal center. All band labels aid referencing in the text and **Tables S2, S3 and S4**. Features associated with the **5II** isomer where a water dimer is bound to the acidic OH are shown in gray in (a) to highlight the spectral behavior of the **5I** isomer.

bars in **Fig. 2**) calculated for the ternary systems, and fall interestingly close to the observed $_{\text{M}}v_{\text{OH}}^{\text{a-w}}$ bands (navy blue in **Fig. 2**). For this scenario of a common (cyclic tetramer) hydration geometry, the calculated $_{\text{M}}v_{\text{OH}}^{\text{a-w}}$ bands in fact are essentially independent of the metal ion size, while the distance

between the metal ion nucleus and the N atom of HNO₃ follow a trend similar to that indicated in **Fig. 1** and tabulated in **Table S4**. As such, the behavior of these isomers can be regarded as a partial cancellation of the electric field from the metal ion by the primary hydration shell.

Although instructive from a conceptual standpoint, the calculated behaviors of the cyclic water tetramer isomers are not representative of the actual structures adopted by the clusters observed in this work. Based on the behavior of the M⁺·(H₂O)_n clusters, for example, it is clear that the solvent structures evolve such that cyclic structures break up for the smaller alkali ions. Several isomers were isolated in the calculations for all of the M⁺ systems and displayed in **Fig. S6**. Indeed, the water molecules in the minimum energy Rb and K clusters feature partially broken cycles with many low-lying isomers. Although the purpose of this work is not to exhaustively survey the many possible isomers available to these systems, there are compelling structural assignments for the Na and Li systems because their spectral patterns in the OH stretching region are particularly simple. The spectra of Cs, Na and Li n=5 clusters are compared in **Fig. 3**, where the former has been analyzed previously in the context of hydration by a cyclic water tetramer as described above.

To unravel the structural information encoded in the pattern of OH stretching fundamentals, it is useful to follow the evolution of bands arising from specific local structural motifs for the various metal ions.⁴⁴ Specifically, the telltale bands signaling a water molecule attached to the acid OH group (in an H-bonding A configuration, see insets to **Fig. 3**) are those corresponding to the symmetric (ν_A^{sym}) and asymmetric (ν_A^{asym}) OH stretching fundamentals at 3651 and 3741 cm⁻¹, respectively. These are highlighted in red in **Fig. 3** and indeed are present in all of the spectra. The interloper between the two red peaks (purple, $\nu_{\text{AD}}^{\text{free}}$) is due to water molecules in AD sites (see inset). For example, the AD feature is much more intense than the A bands in the spectrum of the Cs **5I** isomer (**Fig. 3a**), consistent with four water molecules adopting AD sites in the tetramer ring and one water in an A site bound to the acid OH group. In the Na and Li spectra (**Fig. 3c** and **3e**), on the other hand, the signature A bands are much stronger relative to the AD feature, suggesting that there are fewer water molecules in AD sites relative to those occupying A configurations. This qualitative trend in the red A and purple AD bands is readily explained by the lowest energy Cs, Na and Li isomers depicted in the insets of **Fig. 3**. Specifically, the Li arrangement is derived from the lowest energy Li⁺·(H₂O)₄ structure,³¹ where four water molecules are bound to the ion, all in non-bonded A sites. In the Li⁺·(HNO₃)(H₂O)₅ structure, the four-coordinated hydration motif around the ion is preserved such that the HNO₃(H₂O) moiety is separated from the ion by two bridging AD water molecules. The calculated band pattern for this arrangement (inverted bars in **Fig. 3f**) accounts for the weaker AD band since now there are three A water molecules but only two in AD sites. The two purple bands near 3500 cm⁻¹ in **Fig. 3f** can then be assigned to the symmetric and asymmetric stretches of the two bound OH groups on these AD water molecules ($\nu_{\text{AD}}^{\text{bound}}$) linking the ion to the NO₂ group of the acid. The minimum energy structure of the Na system is similar to this morphology (**Fig. S6**), but features a more complex arrangement in which one of the NO₃ oxygen atoms is retained in the primary hydration shell and the two AD molecules are not optimally aligned to bond onto either the bound or free NO groups on the acid. This more distorted configuration accounts for the single more blue shifted band (purple at 3595 cm⁻¹ in **Fig. 3c**) that is assigned to the single AD linker (inverted purple feature in **Fig. 3d**). The overall picture of the structural evolution from the Cs to Li n=5 clusters is thus seen to be gradual fragmentation of cyclic water motifs for the large ions (Rb and Cs), leading finally to a four-coordinated shell in Li and expulsion of the acid into the second solvation shell. This scenario readily explains the apparent paradox that the smallest ion, in spite of generating the largest local electric field, yields the smallest red-shift in the ${}^{\text{4w}}\nu_{\text{OH}}^{\text{a-w}}$ fundamental.

There are many parameterizations for the dependence of OH stretching frequencies including bond strength, distance between donor and acceptor atoms, and the extended H-bonding network configuration.⁴⁴⁻⁴⁷ As discussed above, a common way to quantify the local environments of OH groups

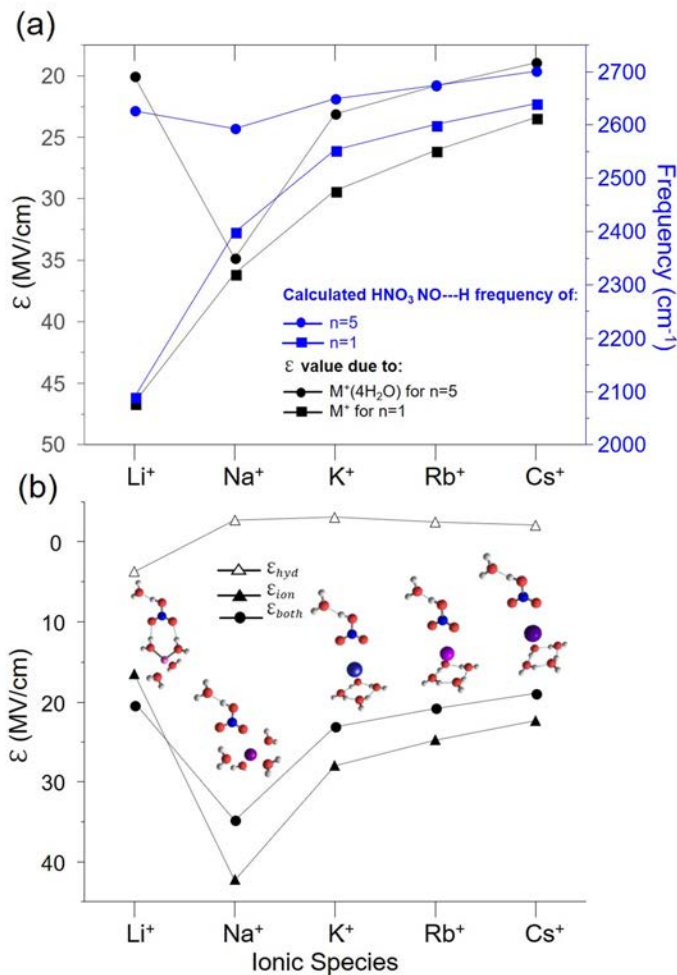


Figure 4. Graph (a) correlates the magnitude of the electric field (left y-axis) with the calculated frequencies of the nitric acid OH stretch (right y-axis) in the ternary complexes ($n=1$) and the $n=5$ series. Graph (b) decomposes the electric field for the $n=5$ clusters, ϵ , into individual contributions from the alkali ion, ϵ_{ion} , and the four water molecules hydrating the cation, ϵ_{hyd} . All results from the B3LYP calculations and calculated harmonic frequencies were scaled by 0.9. Legends for (a) and (b) are included inset along with minimum energy structures for the $M^+(HNO_3)(H_2O)_5$ clusters. Numerical results from these graphs are collected in **Table S5-6**.

that are driving these trends is to consider the role of the local electric field along the acidic OH bond axis, ϵ .⁴⁸⁻⁵⁰ To evaluate the degree to which ϵ can account for the overall v_{OH}^{a-w} behavior observed here, we calculated the contributions to ϵ for the $M^+(HNO_3)(H_2O)$ ternary complexes and for the $n=5$ series, with the results collected in **Fig. 4a**. For the ternary complexes, it is clear that the calculated v_{OH}^{a-w} frequencies (blue solid squares) are strongly correlated with the ϵ values (black solid squares). For the $n=5$ series, although the calculated frequencies (blue solid circles) do not quantitatively recover the local variations in v_{OH}^{a-w} (e.g., the minimum at Rb), they do predict the overall observed trend where there is a minimum value of v_{OH}^{a-w} with decreasing ionic radius and then an increase for the Li system. These calculations also allow for decomposition of the *relative* contributions to the ϵ field (**Fig. 4b**) from the water molecules in the first hydration shell, ϵ_{hyd} , and from the metal ions, ϵ_{ion} . In the simple reaction field picture, for example, the induced solvent orientation dipole opposes the intrinsic field of the metal ion, and as such should yield opposite contributions to ϵ . The contribution from the solvent in the arrangement at the minimum energy structures is indicated by the black open triangles in **Fig. 4b**. The solvent fields indeed oppose that from

the ion for $M = Cs-Na$, but the magnitude of the intrinsic potential suppression from the solvent is actually quite small compared to that from the metal ions, and is indeed even in the same direction for the Li complex. The most important contribution therefore is actually the contribution from the metal ion (black filled triangles in **Fig. 4b**). Another interesting feature of this decomposition is that the Na complex deviates dramatically from this simple local electric field picture. In particular, the calculated

contributions from Na^+ and the four water molecules in the hydration shell to ϵ are much larger than those of the other systems, while the ${}^4w_M v_{\text{OH}}^{a-w}$ frequency displayed by the Na $n=5$ complex is similar to the others. This raises the important contribution from the polarizability anisotropy of the HNO_3 molecule, which comes into play when the docking geometry to the ion is changed. This is the case in the Na structure displayed in **Fig. 3d**, in which the Na^+ binds to the $-\text{NO}_2$ group in a monodentate fashion. The calculated electron distribution in the HNO_3 scaffold is shown in **Table S8** and is indeed significantly different than those found for the bidentate binding motif. It is useful to note that a modified field calculation that includes the contributions from the NO_3 moiety yields ϵ values that are remarkably well correlated with the observed ${}^4w_M v_{\text{OH}}^{a-w}$ trend (see **Fig. S9**). As such, the cluster studies highlight the factors that contribute to frequency shifts in specific bonds, enabling a critical evaluation of the efficacy of simple field models to recover observed behaviors of a strong acid with proximal ions and solvent molecules.

IV. Summary

We have exploited the adventitious formation of $\text{M}^+(\text{HNO}_3)(\text{H}_2\text{O})_5$, $\text{M}=\text{Li}, \text{Na}, \text{K}, \text{Rb}, \text{Cs}$ clusters with a single water molecule attached to the acidic OH of nitric acid to monitor how this linkage evolves with decreasing ionic radius of the alkali metal ion. For the isolated $\text{M}^+(\text{HNO}_3)(\text{H}_2\text{O})$ ternary systems, the strength of the bond to this water molecule is calculated to monotonically increase going from Cs to Li as evidenced by the incremental red shifts in the acid OH stretching band. This effect is traced to the increasing strength of the electrostatic interaction between the smaller ions and the NO_3 moiety, which is reflected in shorter $r(\text{M}^+ \cdots \text{N})$ distances. Contraction of this distance acts to stabilize the incipient NO_3^- conjugate base and thus lower the energy of the intra-cluster proton transfer reaction. The experimental OH stretching frequencies were monitored for the $\text{M}^+(\text{HNO}_3)(\text{H}_2\text{O})_5$ ions with cryogenic IR photodissociation of weakly bound D_2 molecules, and observed to be essentially independent of the metal ion. This behavior reflects the action of the four water molecules in the primary hydration shell around the ion. Two distinct contributions to this interaction are elucidated by analysis of the patterns of bands in the OH stretching region. One contribution is the ion-driven reorientation of these water molecules, which acts to counter the electric field from the ions and is thus a molecular level articulation of dielectric screening in a continuum picture. The second way that the HNO_3 acidity is affected is by ion-induced restructuring of the hydration shell such that the $\text{HNO}_3/\text{H}_2\text{O}$ motif is displaced into the second solvation shell around the metal ion as the four water molecules bind more strongly to the smaller ions. The latter effect accounts for the fact that the HNO_3 bond to the water molecule is weakest in the Li system despite the fact that the smallest ion delivers the largest local electric field. Although the simple field cancellation picture qualitatively captures the calculated behavior of the acidic OH frequency shifts when a common hydration is enforced, this procedure fails when the local binding of the metal to the $-\text{NO}_2$ changes from bidentate to monodentate in the Na complex. The variation in the strength of the $\text{HNO}_3/\text{H}_2\text{O}$ interaction also yields a systematic evaluation of the anti-correlation between the frequencies of the acid OH stretching and bending fundamentals.

V. Supporting Information

The Supporting Information, which includes detailed experimental and computational data, is available free of charge on the ACS Publications website.

VI. Authors' Contributions

S.M., T.K., and M.A.J. conceptualized the experiment and collected experimental data. S.M. identified various local minima for all computed structures. T.H.C, R.M.H., K.D.J., and A.B.M. refined and extracted computational details. S.M., T.K., K.D.J, A.B.M., and M.A.J. wrote the manuscript.

VII. Acknowledgements

MAJ, ABM and KDJ gratefully acknowledge the Department of Energy through the condensed phase and interfacial molecular science (CPIMS) program under grants DE-SC0021012, DE-SC0021081, and DE-SC0021065, respectively, for support of this work.

VIII. Author information

Corresponding Authors

*E-mail: jordan@pitt.edu (K.D.J.)

*E-mail: abmccoy@uw.edu (A.B.M)

*E-mail: mark.johnson@yale.edumark (M.A.J.).

ORCID

Sayoni Mitra: 0000-0003-4526-730X

Thien Khuu: 0000-0003-0386-2450

Tae Hoon Choi: 0000-0002-2009-8557

Rachel M. Huchmala: 0000-0002-3548-1655

Kenneth D. Jordan: 0000-0001-9178-6771

Anne B. McCoy: 0000-0001-6851-6634

Mark A. Johnson: 0000-0002-1492-6993

IX. Author Declaration

The authors declare no competing financial or conflict of interest.

X. References

1. Lewis, T.; Winter, B.; Stern, A. C.; Baer, M. D.; Mundy, C. J.; Tobias, D. J.; Hemminger, J. C. Does Nitric Acid Dissociate at the Aqueous Solution Surface? *J. Phys. Chem. C* **2011**, *115* (43), 21183-21190.
2. Bianco, R.; Wang, S. Z.; Hynes, J. T. Infrared Signatures of HNO₃ and NO₃⁻ at a Model Aqueous Surface: A Theoretical Study. *Journal of Physical Chemistry A* **2008**, *112* (39), 9467-9476.
3. Shamay, E. S.; Buch, V.; Parrinello, M.; Richmond, G. L. At the Water's Edge: Nitric Acid as a Weak Acid. *J. Am. Chem. Soc.* **2007**, *129* (43), 12910-12911.
4. Gilligan, J. J.; Castleman, A. W. Acid Dissolution by Aqueous Surfaces and Ice: Insights from a Study of Water Cluster Ions. *Journal of Physical Chemistry A* **2001**, *105* (23), 5601-5605.

5. Yang, H. S.; Finlayson-Pitts, B. J. Infrared spectroscopic studies of binary solutions of nitric acid and water and ternary solutions of nitric acid, sulfuric acid, and water at room temperature: Evidence for molecular nitric acid at the surface. *Journal of Physical Chemistry A* **2001**, *105* (10), 1890-1896.
6. Soule, M. C. K.; Blower, P. G.; Richmond, G. L. Nonlinear vibrational spectroscopic studies of the adsorption and speciation of nitric acid at the vapor/acid solution interface. *Journal of Physical Chemistry A* **2007**, *111* (17), 3349-3357.
7. Kuo, M. H.; David, A.; Kamelamela, N.; White, M.; Shultz, M. J. Nitric acid - Water interaction probed via isolation in carbon tetrachloride. *J Phys Chem C* **2007**, *111* (25), 8827-8831.
8. Schnitzer, C.; Baldelli, S.; Campbell, D. J.; Shultz, M. J. Sum frequency generation of O-H vibrations on the surface of H₂O/HNO₃ solutions and liquid HNO₃. *Journal of Physical Chemistry A* **1999**, *103* (32), 6383-6386.
9. Wang, S. Z.; Bianco, R.; Hynes, J. T. An Atmospherically Relevant Acid: HNO₃. *Computational and Theoretical Chemistry* **2011**, *965* (2-3), 340-345.
10. Baer, M. D.; Tobias, D. J.; Mundy, C. J. Investigation of Interfacial and Bulk Dissociation of HBr, HCl, and HNO₃ Using Density Functional Theory-Based Molecular Dynamics Simulations. *Journal of Physical Chemistry C* **2014**, *118* (50), 29412-29420.
11. Petersen, P. B.; Saykally, R. J. Is the liquid water surface basic or acidic? Macroscopic vs. molecular-scale investigations. *Chem. Phys. Lett.* **2008**, *458* (4-6), 255-261.
12. Mishra, H.; Enami, S.; Nielsen, R. J.; Hoffmann, M. R.; Goddard, W. A.; Colussi, A. J. Anions dramatically enhance proton transfer through aqueous interfaces. *Proc. Natl. Acad. Sci. USA* **2012**, *109* (26), 10228-10232.
13. Mishra, H.; Nielsen, R. J.; Enami, S.; Hoffmann, M. R.; Colussi, A. J.; Goddard III, W. A. Quantum chemical insights into the dissociation of nitric acid on the surface of aqueous electrolytes. *International Journal of Quantum Chemistry* **2013**, *113* (4), 413-417.
14. Choi, J. H.; Kuwata, K. T.; Haas, B. M.; Cao, Y. B.; Johnson, M. S.; Okumura, M. Vibrational spectroscopy of NO⁺(H₂O)_n: Evidence for the intracuster reaction NO⁺(H₂O)_n → H₃O⁺(H₂O)_{n-2} (HONO) at n ≥ 4. *J. Chem. Phys.* **1994**, *100* (10), 7153-7165.
15. Mitra, S.; Duong, C. H.; McCaslin, L. M.; Gerber, R. B.; Johnson, M. A. Isomer-Specific Cryogenic Ion Vibrational Spectroscopy of the D₂-Tagged Cs⁺·(HNO₃)(H₂O)_(n = 0-2) Complexes: Ion-Driven Enhancement of the Acidic H-Bond to Water. *Phys. Chem. Chem. Phys.* **2020**, *22* (8), 4501-4507.
16. Mitra, S.; Yang, N.; McCaslin, L. M.; Gerber, R. B.; Johnson, M. A. Size-Dependent Onset of Nitric Acid Dissociation in Cs⁺·(HNO₃)(H₂O)_{n=0-11} Clusters at 20 K. *Journal of Physical Chemistry Letters* **2021**, *12* (13), 3335-3342.
17. Wolk, A. B.; Leavitt, C. M.; Garand, E.; Johnson, M. A. Cryogenic Ion Chemistry and Spectroscopy. *Accounts Chem Res* **2014**, *47* (1), 202-210.
18. Onsager, L. Deviations from Ohm's Law in Weak Electrolytes. *Journal of Chemical Physics* **1934**, *2* (9).
19. Zatula, A. S.; Ryding, M. J.; Andersson, P. U.; Uggerud, E. Proton Mobility and Stability of Water Clusters Containing Alkali Metal Ions. *Int. J. Mass Spec.* **2012**, *330*, 191-199.
20. Roscioli, J. R.; McCunn, L. R.; Johnson, M. A. Quantum Structure of the Intermolecular Proton Bond. *Science* **2007**, *316*, 249-254.
21. Wolk, A. B.; Leavitt, C. M.; Garand, E.; Johnson, M. A. Cryogenic Ion Chemistry and Spectroscopy. *Acc. Chem. Res.* **2014**, *47* (1), 202-210.
22. Yanai, T.; Tew, D. P.; Handy, N. C. A new hybrid exchange-correlation functional using the Coulomb-attenuating method (CAM-B3LYP). *Chemical Physics Letters* **2004**, *393* (1-3), 51-57.
23. Lee, C. T.; Yang, W. T.; Parr, R. G. Development of the Colle-Salvetti Correlation-Energy Formula into a Functional of the Electron-Density. *Phys. Rev. B* **1988**, *37* (2), 785-789.
24. Zhang, X.; Mereand, E. L.; Castleman, A. W., Jr. Reactions of Water Cluster Ions with Nitric Acid. *J. Phys. Chem.* **1994**, *98*, 3554-3557.
25. Dzidic, I.; Kebarle, P. Hydration of Alkali Ions in Gas Phase - Enthalpies and Entropies of Reactions M⁺(H₂O)_{n-1}+H₂O = M⁺(H₂O)_n. *J Phys Chem-Us* **1970**, *74* (7), 1466-&

26. Glendening, E. D.; Feller, D. Cation Water Interactions - the $M^+(H_2O)_n$ Clusters for Alkali-Metals, $M=Li, Na, K, Rb,$ and Cs . *J Phys Chem-Us* **1995**, *99* (10), 3060-3067.
27. Duong, C. H.; Gorlova, O.; Yang, N.; Kelleher, P. J.; Johnson, M. A.; McCoy, A. B.; Yu, Q.; Bowman, J. M. Disentangling the Complex Vibrational Spectrum of the Protonated Water Trimer, $H^+(H_2O)_3$, with Two-Color IR-IR Photodissociation of the Bare Ion and Anharmonic VSCF/VCI Theory. *Journal of Physical Chemistry Letters* **2017**, *8* (16), 3782-3789.
28. Yang, N.; Edington, S. C.; Choi, T. H.; Henderson, E. V.; Heindel, J. P.; Xantheas, S. S.; Jordan, K. D.; Johnson, M. A. Mapping the temperature-dependent and network site-specific onset of spectral diffusion at the surface of a water cluster cage. *P. Natl. Acad. Sci. USA* **2020**, *117* (42), 26047-26052.
29. McCoy, A. B.; Guasco, T. L.; Leavitt, C. M.; Olesen, S. G.; Johnson, M. A. Vibrational Manifestations of Strong Non-Condon Effects in the $H_3O^+ \cdot X_3$ ($X = Ar, N_2, CH_4, H_2O$) Complexes: A Possible Explanation for the Intensity in the "Association Band" in the Vibrational Spectrum of Water. *Phys. Chem. Chem. Phys.* **2012**, *14* (20), 7205-7214.
30. Seki, T.; Chiang, K. Y.; Yu, C. C.; Yu, X. Q.; Okuno, M.; Hunger, J.; Nagata, Y.; Bonn, M. The Bending Mode of Water: A Powerful Probe for Hydrogen Bond Structure of Aqueous Systems. *Journal of Physical Chemistry Letters* **2020**, *11* (19), 8459-8469.
31. Miller, D. J.; Lisy, J. M. Hydrated Alkali-Metal Cations: Infrared Spectroscopy and ab Initio Calculations of $M^+(H_2O)_{x=2-5}$ Ar cluster ions for $M = Li, Na, K,$ and Cs . *J. Am. Chem. Soc.* **2008**, *130* (46), 15381-15392.
32. Miller, D. J.; Lisy, J. M. Entropic Effects on Hydrated Alkali-Metal Cations: Infrared Spectroscopy and ab Initio Calculations of $M^+(H_2O)_{x=2-5}$ Cluster Ions for $M = Li, Na, K,$ and Cs . *J. Am. Chem. Soc.* **2008**, *130* (46), 15393-15404.
33. Fournier, J. A.; Wolke, C. T.; Johnson, C. J.; Johnson, M. A.; Heine, N.; Gewinner, S.; Schollkopf, W.; Esser, T. K.; Fagiani, M. R.; Knorke, H.; Asmis, K. R. Site-Specific Vibrational Spectral Signatures of Water Molecules in the Magic $H_3O^+(H_2O)_{20}$ and $Cs^+(H_2O)_{20}$ Clusters. *Proc. Natl. Acad. Sci.* **2014**, *111* (51), 18132-18137.
34. Keutsch, F. N.; Saykally, R. J. Water clusters: untangling the mysteries of the liquid, one molecule at a time. *Proc. Natl. Acad. Sci.* **2001**, *98*, 10533-10540.
35. Pribble, R. N.; Zwier, T. S. Size-specific Infrared Spectra of Benzene- $(H_2O)_n$ clusters ($n=1$ through 7): Evidence for Noncyclic $(H_2O)_n$ Structures. *Science* **1994**, *265*, 75-79.
36. Perez, C.; Muckle, M. T.; Zaleski, D. P.; Seifert, N. A.; Temelso, B.; Shields, G. C.; Kisiel, Z.; Pate, B. H. Structures of Cage, Prism, and Book Isomers of Water Hexamer from Broadband Rotational Spectroscopy. *Science* **2012**, *336* (6083), 897-901.
37. Mahler, J.; Persson, I. A Study of the Hydration of the Alkali Metal Ions in Aqueous Solution. *Inorganic Chemistry* **2012**, *51* (1), 425-438.
38. Cruzan, J. D.; Brown, M. G.; Liu, K.; Braly, L. B.; Saykally, R. J. The far-infrared vibration-rotation-tunneling spectrum of the water tetramer-d8. *The Journal of Chemical Physics* **1996**, *105* (16), 6634-6644.
39. Denton, J. K.; Kelleher, P. J.; Johnson, M. A.; Baer, M. D.; Kathmann, S. M.; Mundy, C. J.; Wellen Rudd, B. A.; Allen, H. C.; Choi, T.; Jordan, K. D. Molecular-Level Origin of the Carboxylate Head Group Response to Divalent Metal Ion Complexation at the Air-Water Interface. *Proc. Natl. Acad. Sci.* **2019**, *116* (30), 14874-14880.
40. Debye, P.; Huckel, E. The theory of the electrolyte II - The border law for electrical conductivity. *Phys Z* **1923**, *24*, 305-325.
41. Debye, P.; Huckel, E. The theory of electrolytes I. The lowering of the freezing point and related occurrences. *Phys Z* **1923**, *24*, 185-206.
42. Levin, Y. Electrostatic correlations: from plasma to biology. *Rep Prog Phys* **2002**, *65* (11), 1577-1632.
43. Laidler, K. J.; Pegis, C. The Influence of Dielectric Saturation on the Thermodynamic Properties of Aqueous Ions. *Proceedings of the Royal Society of London Series a-Mathematical and Physical Sciences* **1957**, *241* (1224), 80-92.

44. Yang, N.; Khuu, T.; Mitra, S.; Duong, C. H.; Johnson, M. A.; DiRisio, R. J.; McCoy, A. B.; Miliordos, E.; Xantheas, S. S. Isolating the Contributions of Specific Network Sites to the Diffuse Vibrational Spectrum of Interfacial Water with Isotopomer-Selective Spectroscopy of Cold Clusters. *Journal of Physical Chemistry A* **2020**, *124* (50), 10393-10406.
45. Ohno, K.; Okimura, M.; Akai, N.; Katsumoto, Y. The effect of cooperative hydrogen bonding on the OH stretching-band shift for water clusters studied by matrix-isolation infrared spectroscopy and density functional theory. *Phys Chem Chem Phys* **2005**, *7* (16), 3005-3014.
46. Tainter, C. J.; Skinner, J. L. The Water Hexamer: Three-Body Interactions, Structures, Energetics, and OH-Stretch Spectroscopy at Finite Temperature. *Journal of Chemical Physics* **2012**, *137* (10).
47. Boyer, M. A.; Marsalek, O.; Heindel, J. P.; Markland, T. E.; McCoy, A. B.; Xantheas, S. S. Beyond Badger's Rule: The Origins and Generality of the Structure-Spectra Relationship of Aqueous Hydrogen Bonds. *The Journal of Physical Chemistry Letters* **2019**, *10* (5), 918-924.
48. Hermansson, K. Electric-field effects on the OH vibrational frequency and infrared absorption intensity for water. *J. Chem. Phys.* **1993**, *99*, 861-868.
49. Gruenbaum, S. M.; Tainter, C. J.; Shi, L.; Ni, Y.; Skinner, J. L. Robustness of Frequency, Transition Dipole, and Coupling Maps for Water Vibrational Spectroscopy. *J. Chem. Theory Comput.* **2013**, *9* (7), 3109-3117.
50. Kebede, G. G.; Mitev, P. D.; Briels, W. J.; Hermansson, K. Red-shifting and blue-shifting OH groups on metal oxide surfaces - towards a unified picture. *Phys Chem Chem Phys* **2018**, *20* (18), 12678-12687.